PERGAMON

Chemical Engineering Science 56 (2001) 503–512

Chemical Engineering Science

www.elsevier.nl/locate/ces

Eulerian simulations for determination of the axial dispersion of liquid and gas phases in bubble columns operating in the churn-turbulent regime

J. M. van Baten, R. Krishna*

Department of Chemical Engineering, University of Amsterdam, Nieuwe Achtergracht 166, 1018 WV Amsterdam, Netherlands

Abstract

Fully three-dimensional (3D) transient simulations using computational fluid dynamics (CFD) have been carried out for bubble columns operating in the churn-turbulent flow regime. The bubble column is considered to be made up of three phases: (1) liquid, (2) "small" bubbles and (3) "large" bubbles and the Eulerian description is used for each of these phases. Interactions between both bubble populations and the liquid are taken into account in terms of momentum exchange, or drag, coefficients, which differ for the "small" and "large" bubbles. Water and Tellus oil, with a viscosity 75 times that of water, were used as liquid phase and air as gaseous phase. The transient tracer responses in the gas and liquid phases were monitored at three different stations in the column and the results analysed in terms of a one-dimensional axial dispersion model. The 3D simulation results for radial distribution of liquid velocity ($V_L(r)$), centre-line liquid velocity ($V_L(0)$), axial dispersion coefficients of the liquid ($D_{ax,L}$) and gas ($D_{ax,G}$) phases, for columns of 0.174, 0.38 and 0.63 m in diameter were compared with experimental data generated in our laboratories and also literature correlations. There is good agreement between the values of $V_L(r)$, $V_L(0)$ and $D_{ax,L}$ from 3D simulations with measured experimental data. The axial dispersion coefficient of the small bubble population was almost the same as that of $D_{ax,L}$, whereas the dispersion of the large bubbles is significantly lower in magnitude. It is concluded that 3D transient Eulerian simulations are potent tools for investigating the gas and liquid residence time distributions and have potential use as scale-up tools.

Keywords: Bubble columns; Large bubbles; Small bubbles; Churn-turbulent flow regime; Radial velocity profiles; Computational fluid dynamics; Axial dispersion

1. Introduction

Bubble column reactors are attracting increasing academic and industrial research interest in view of the many potential applications in natural gas conversion technologies (Krishna, Ellenberger & Sie, 1996; Krishna & Sie, 2000). For the Fischer–Tropsch synthesis, for example, the bubble column slurry reactor is the most attractive reactor choice (Sie & Krishna, 1999). In view of the large gas throughputs involved in the process, the bubble column needs to be operated at high superficial gas velocities, typically with $U = 0.2$–0.4 m/s, in the churn-turbulent flow regime. For commercial viability of the Fischer–Tropsch process, gas-phase conversions in excess of 90% must be achieved (Maretto & Krishna, 1999). This requirement places severe demands on our capabilities to predict the hydrodynamic parameters (hold-up, mass transfer, axial dispersion of gas and liquid phases) for commercial scale reactors that could have diameters exceeding 6 m. Bearing in mind that cold-flow hydrodynamics and mass transfer studies are often carried out in laboratory scale reactors with diameter smaller than say 0.5 m, there is a need for a systematic and scientific approach to scale up (Krishna, 2000).

In this work we use computational fluid dynamics (CFD), in the Eulerian framework, to describe the hydrodynamics of bubble columns reactors operating in the churn-turbulent flow regime. Eulerian simulations are used to estimate the gas and liquid-phase dispersion characteristics. Validation of the Eulerian simulations is sought by comparison with the extensive data set generated by our group in earlier work (Krishna, Urseanu, van Baten & Ellenberger, 1999b, 2000; Krishna, van Baten

* Corresponding author. Tel.: +31-20-525-7007; fax: +31-20-525-5604.

E-mail address: krishna@its.chem.uva.nl (R. Krishna).

0009-2509/01/$ - see front matter
PII: S0009-2509(00)00254-2

& Urseanu, 2000). The basic philosophy of our approach is that once Eulerian simulations have been validated on a variety of scales for a variety of systems, these could be used with some confidence as predictive tools for commercial scale reactors.

2. Development of CFD model

For the homogeneous regime of operation of bubble columns, a more or less uniform bubble size is obtained and many CFD approaches have been successfully developed to cater for this regime of operation using the Eulerian description for the gas and liquid phases (Jakobsen, Sannæs, Grevskott & Svendsen, 1997; Sanyal, Vasquez, Roy & Dudukovic, 1999; Sokolichin & Eigenberger, 1999).

In the churn-turbulent regime of operation the bubble sizes vary over a wide range between 1 and 50 mm depending on the operating conditions and phase properties (De Swart, Van Vliet & Krishna, 1996). The rise characteristics of the bubbles depend on its size and liquid-phase properties (Krishna & van Baten, 1999). Our approach for modelling purposes is to assume that in the churn-turbulent flow regime we have two distinct bubble classes: "small" and "large" (see Fig. 1(a)). For air–water systems the small bubbles are typically in the 3–6 mm size range and are ellipsoidal in shape and the large bubbles are in the 15–50 mm size range and correspond to the spherical cap bubbles. For each of the three phases shown in Fig. 1(a) the volume-averaged mass and momentum conservation equations in the Eulerian framework are given by Eqs. (1) and (2) in Table 1. For the continuous liquid phase, the turbulent contribution to the stress tensor is evaluated by means of k–ε model, using standard single-phase parameters given in Eq. (3). The applicability of the k–ε model has been considered in detail by Sokolichin and Eigenberger (1999). No

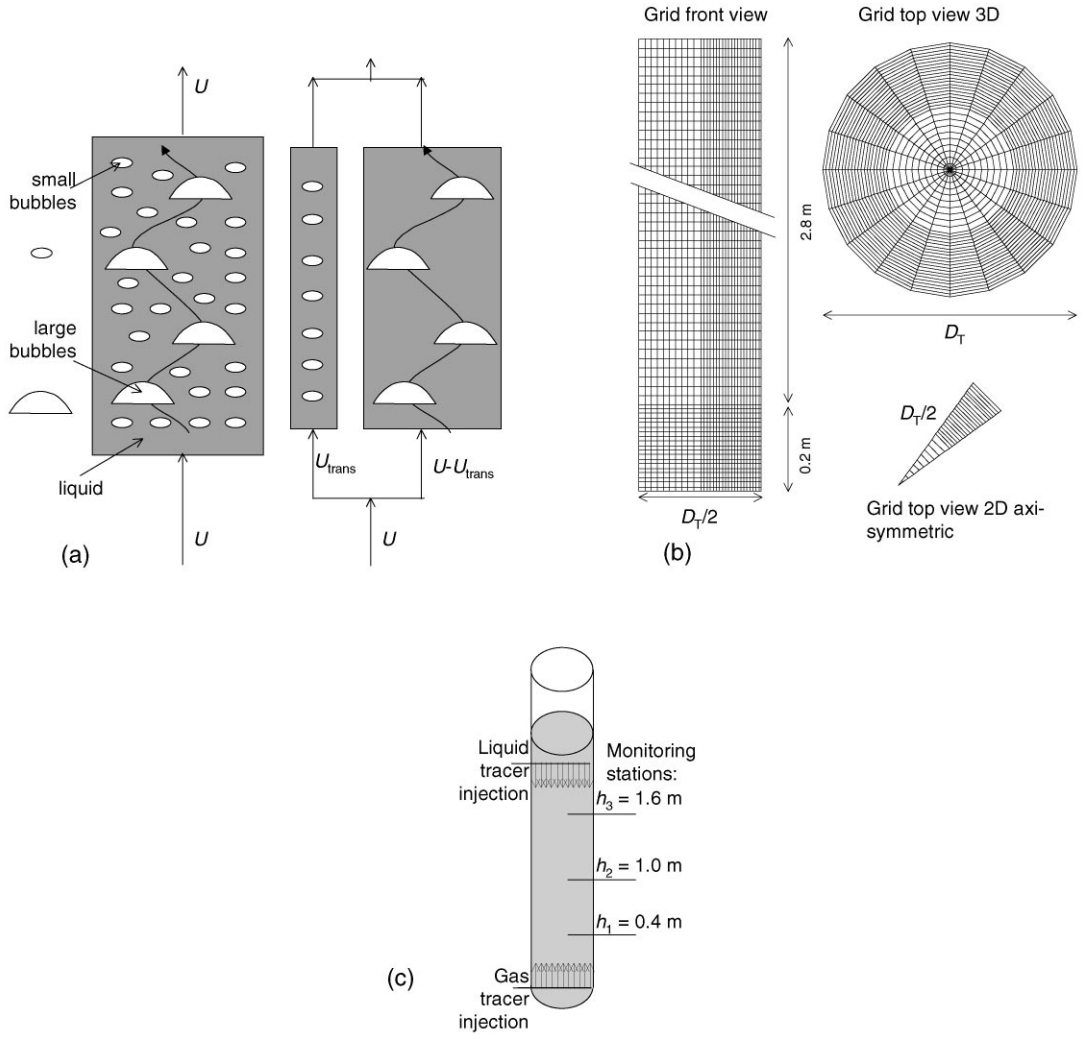

Fig. 1. (a) Three-phase model for bubble columns operating in the churn-turbulent flow regime. (b) Computational grid for 3D and 2D axi-symmetric simulations. (c) Liquid- and gas-phase tracer injection strategies in Eulerian simulations. The tracer concentrations are monitored at three stations over the entire cross-section.

Table 1
Model equations for bubble column reactors operating in the churn-turbulent flow regime

Equation description and number	Equation
Eulerian simulation model	
Volume-averaged mass conservation Eq. (1)	$\frac{\partial(\varepsilon_k\rho_k)}{\partial t} + \nabla\bullet(\rho_k\varepsilon_k\mathbf{u}_k) = 0$
Volume-averaged momentum conservation Eq. (2)	$\frac{\partial(\rho_k\varepsilon_k\mathbf{u}_k)}{\partial t} + \nabla\bullet(\rho_k\varepsilon_k\mathbf{u}_k\mathbf{u}_k - \mu_k\varepsilon_k(\nabla\mathbf{u}_k + (\nabla\mathbf{u}_k)^{\mathrm{T}})) = -\varepsilon_k\nabla p + \mathbf{M}_{kl} + \rho_k\mathbf{g}$
k–ε turbulence parameters, Eq. (3)	$C_\mu = 0.09, C_{1\varepsilon} = 1.44, C_{2\varepsilon} = 1.92, \sigma_k = 1$ and $\sigma_\varepsilon = 1.3$
Interphase momentum exchange between large bubble phase (subscript b) and liquid (subscript L), Eq. (4)	$\mathbf{M}_{L,b} = \frac{3}{4}\rho_L\frac{\varepsilon_b}{d_b}C_D(\mathbf{u}_b - \mathbf{u}_L)\lvert\mathbf{u}_b - \mathbf{u}_L\rvert$
Drag coefficient, Eq. (5)	$C_D = \frac{4}{3}\frac{\rho_L - \rho_G}{\rho_L}gd_b\frac{1}{V_b^2}$
"*Small*" *bubbles*	
Harmathy (1960) correlation for rise velocity of small bubbles, Eq. (6)	$V_{b,\mathrm{small}} = 1.53\left(\frac{\sigma g}{\rho_L}\right)^{0.25}$
Mendelson (1967) correlation for rise velocity of small bubbles, Eq. (7)	$V_{b,\mathrm{small}} = \sqrt{2\sigma/\rho_L d_b + gd_b/2}$
"*Large*" *bubbles*	
Velocity of large bubble swarms, Eq. (8)	$V_b = 0.71\sqrt{gd_b}(SF)(AF)$
Scale factor, Eq. (9)	$\mathrm{SF} = 1$ for $d_b/D_T < 0.125$; $\mathrm{SF} = 1.13\exp(-d_b/D_T)$ for $0.125 < d_b/D_T < 0.6$; $\mathrm{SF} = 0.496\sqrt{D_T/d_b}$ for $d_b/D_T > 0.6$
Acceleration factor, Eq. (10)	$\mathrm{AF} = 2.73 + 4.505(U - U_{\mathrm{trans}})$; for water $\mathrm{AF} = 2.25 + 4.09(U - U_{df})$; for Tellus oil
Average size of large bubbles for both air–water and air–Tellus oil systems, Eq. (11)	$d_b = 0.069(U - U_{\mathrm{trans}})^{0.376}$
Axial dispersion of tracer within liquid phase	
One-dimensional conservation equation for (transient) tracer mass concentration c_L in the liquid phase, Eq. (12)	$\frac{\partial c_L}{\partial t} = D_{\mathrm{ax},L}\frac{\partial^2 c_L}{\partial x^2}$
Analytical solution, given in Deckwer (1992), for tracer concentration c_L at distance x from the point of tracer injection (Dirac delta function) in a column of length L, Eq. (13)	$\frac{c_L(t,x)}{c_L(\infty)} = 1 + 2\sum_{n=1}^{\infty}\cos(n\pi x/L)\exp\left(-D_{\mathrm{ax},L}(\frac{\pi n}{L})^2 t\right)$
Axial dispersion of tracer within gas phase	
One-dimensional conservation equation for (transient) tracer mass concentration c_G in the gas phase, Eq. (14)	$\frac{\partial c_G}{\partial t} = D_{\mathrm{ax},G}\frac{\partial^2 c_G}{\partial x^2} - u_G\frac{\partial c_G}{\partial x}$
Analytical solution, given in Westerterp, van Swaaij and Beenackers (1984), for tracer concentration c_L at distance x from the point of tracer injection (Dirac delta function), Eq. (15)	$\frac{c_G}{c_G(0)} = \sqrt{\frac{Pe}{\pi\theta}}\exp\left(\frac{-\frac{1}{4}Pe(1-\theta)^2}{\theta}\right) - Pe\exp(Pe)\cdot\frac{\mathrm{erfc}\left(\sqrt{\frac{Pe}{\theta}}\frac{1+\theta}{2}\right)}{2}$ $Pe = \frac{xu_G}{D_{\mathrm{ax},G}}, \quad \theta = \frac{tu_G}{x}$
Physical properties used in the simulations	
Air: (density, $\rho_G = 1.29$ kg/m^3; viscosity, $\mu_G = 0.000017$ Pa s); Water: (density, $\rho_L = 998$ kg/m^3; viscosity, $\mu_L = 0.001$ Pa s); Tellus oil: (density, $\rho_L = 862$ kg/m^3; viscosity, $\mu_L = 0.075$ Pa s)	

turbulence model is used for calculating the velocity fields inside the dispersed "small" and "large" bubble phases.

The momentum exchange between either bubble-phase (subscript b) and liquid-phase (subscript L) phases is given by Eq. (4). The liquid phase exchanges momentum with both the "small" and "large" bubble phases. No interchange between the "small" and "large" bubble phases have been included in the present model and each of the dispersed bubble phases exchanges momentum only with the liquid phase. The neglect of the interactions between the small and large bubble populations is due to the conclusion reached by Vermeer and Krishna (1981). The interphase drag coefficient is calculated from Eq. (5) where V_b is the rise velocity of the appropriate bubble population. We have only included the drag force contribution to $\mathbf{M}_{L,b}$, in keeping with the works of Sanyal et al. (1999) and Sokolichin and Eigenberger (1999). The added mass force has been ignored in the present analysis. The reason for this neglect is because the focus of the simulations and experiments in this work is on the churn-turbulent flow regime. The distinguishing feature of this regime is the existence of large fast-rising bubbles. These large bubbles do not have a closed wake and the concept of added mass is not applicable. The small bubbles on the other hand do have a closed wake. However, in the churn-turbulent flow regime these bubbles suffer strong recirculations, moving downwards near the wall region. Inclusion of the added mass contributions to the small bubbles led to severe convergence difficulties. The added mass contributions were therefore omitted. Lift forces are also ignored in the present analysis because of the uncertainty in assigning values of the lift coefficients to the small and large bubbles. For the large bubbles, for which Eö > 40 holds, literature data suggest the use of a negative lift coefficient, whereas for small bubbles for which typically Eö $= 2$, the lift coefficient is positive (Jakobsen et al., 1997).

The diameter of the "small" bubbles was chosen to be 4 mm in all the simulations for the air–water system. The rise velocity of air bubbles is practically independent of bubble diameter in this size range and the Harmathy (1960) equation for the rise velocity, Eq. (6), is used in the simulation results presented in this paper. An alternative, comparable correlation for the small bubble rise velocity is that of Mendelson (1967), Eq. (7).

For the air–Tellus oil system, our dynamic gas disengagement experiments carried out earlier (Krishna, Urseanu, Van Baten & Ellenberger, 1999a) showed that the hold-up of the small bubble population was less than 2% and so we decided to ignore this presence of the small bubbles altogether in the CFD calculations. This neglect is achieved by setting $U_{\text{trans}} = 0$. The hydrodynamics of air–Tellus oil system corresponds roughly to a situation in which large (spherical cap) bubbles rise through the column in a chain.

From the Reilly, Scott, De Bruijn and MacIntyre (1994) correlation, it was determined that the superficial gas velocity at the regime transition point for air–water $U_{\text{trans}} = 0.034$ m/s. For air–water operation at $U \leqslant 0.034$ m/s, homogeneous bubbly flow regime was taken to prevail. Therefore, only two phases, small bubbles and liquid are present. For churn-turbulent operation at $U > 0.034$ m/s, the complete three-phase model was invoked. Following the model of Krishna and Ellenberger (1996) we assume that in the churn-turbulent flow regime the superficial gas velocity through the small bubble phase is $U_{\text{trans}} = 0.034$ m/s (see Fig. 1(a)). The remainder of the gas $(U - U_{\text{trans}})$ was taken to rise up the column in the form of large bubbles. This implies that at the distributor the "large" bubbles constitute a fraction $(U - U_{\text{trans}})/U$ of the total incoming volumetric flow, whereas the "small" bubble constitute a fraction (U_{trans}/U) of the total incoming flow. Strictly speaking, U_{trans} is a model parameter and its choice has a significant increasing effect on the small bubble hold-up but its influence on the the centre-line velocity is negligible (Krishna et al., 1999b).

The large bubble rise velocity was modelled using the approach developed by Krishna et al. (1999a) which introduces an acceleration factor AF into the Collins (1967) relation for the rise of a single spherical cap bubble. The expressions developed for the large bubble size and acceleration factor for air–water and air–Tellus oil systems, summarised in Eqs. (8)–(11), are used in this work for estimation of the drag coefficient for the large bubble phase.

A commercial CFD package CFX 4.2 of AEA Technology, Harwell, UK, was used to solve the equations of continuity and momentum. This package is a finite volume solver, using body-fitted grids. The grids are non-staggered and all variables are evaluated at the cell centres. An improved version of the Rhie–Chow algorithm is used to calculate the velocity at the cell faces. The pressure–velocity coupling is obtained using the SIMPLEC algorithm. For the convective terms in Eqs. (1) and (2) hybrid differencing was used. A fully implicit backward differencing scheme was used for the time integration.

The computational grid used for a 3 m tall column, is shown in Fig. 1(b). Anticipating steeper velocity gradients near the wall region and in the bottom portion of the column, a non-uniform grid was used. In the radial direction 30 grid cells were used, 10 grid cells in the central core and 20 grid cells towards the wall region. In the axial direction, the first 0.2 m bottom portion of the column consisted of 10 mm cells and the remainder 2.8 m height consisted of 20 mm cells. The total number of cells in the azimuthal direction was 20. The total number of cells was $30 \times 160 \times 20 = 96\,000$. Identical grid was used for the 0.174, 0.38 and 0.63 m diameter columns. In some simulations two-dimensional (2D) axi-symmetry was

Table 2
Column configurations, systems, operating conditions and grid details of CFD simulations[a]

Liquid phase	Column diameter D_T (m)	Column height (m)	Initial liquid height (m)	Observation height (m)	Superficial gas velocity, U/(m/s)
Water	0.174	3	1.8,2	1.6	0.02,0.034,0.09,0.16,0.23,0.27,0.3
Water	0.174	3	1.8	1.6	0.23
Water	0.38	3	1.8	1.6	0.23,0.285,0.3
Water	0.63	3	1.8	1.6	0.23,0.285,0.3
Tellus oil	0.38	2	1.4	1.4	0.23

[a]For operation at $U < U_{trans}$, homogeneous bubbly flow regime was taken to prevail. For operation at $U > U_{trans}$, the complete three-phase model was invoked. The large bubble phase was injected over the central 13 of the 30 grid cells in the radial direction. The small bubble phase was injected over the central 24 of the 30 grid cells. The reported liquid velocity profiles are at the observation heights reported below. The reported values of the total gas hold-up refer to the fractional gas volume below this observation height.

assumed. The large bubbles were injected in the central core of the column, in the central 13 of the 30 cells in the radial direction. The small bubbles were distributed over the central 24 of the 30 cells in the radial direction.

A number of fully 3D simulations and 2D axi-symmetric simulations were carried out for the 0.1, 0.14, 0.174, 0.19, 0.38 and 0.63 m diameter columns operating with air–water and air–Tellus oil systems (see Table 2). The column was initial filled with pure liquid up to a height of say 1.8 m and the transient simulations were started with gas injection at time $t = 0$ s at the distributor plate. A typical time-stepping strategy for a 3D simulation was: 100 steps at 5×10^{-4} s, 100 steps at 1×10^{-3} s, 19 800 steps at 3×10^{-3} s. Running on a Silicon Graphics Power Challenge machine employing three R10000 processors in parallel, this simulation took about 8 weeks to complete 20 000 time steps. At the end of 11 000 time steps, sufficient to attain quasi-steady-state conditions, tracer was injected into the entering gas phase, uniformly over the whole cross-section, just above the bottom grid. At the same time step, liquid tracer was injected near the top of the dispersion, typically 2 m above the distributor plate. The transient responses of the gas and liquid phases were monitored over the entire grid cross-section at three monitoring stations, $h = 0.4$,1 and 1.6 m above the distributor plate.

Further details of the 2D and 3D simulations, including animations of column start-up dynamics are available on our web sites: http://ct-cr4.chem.uva.nl/euler2D and http://ct-cr4.chem.uva.nl/euler3D. A comparison of the 2D and 3D animations for 0.38 m diameter column operating at $U = 0.23$ m/s is available on our web site: http://ct-cr4.chem.uva.nl/oil-water.

3. Eulerian simulations vs. experiments

The 3D simulation shows chaotic behaviour and this is illustrated by the snapshots of the liquid velocity and bubble hold-up profiles, at an arbitrary vertical plane, at the three monitoring stations for three time steps, separated by 2.5 s (see Figs. 2(a)–(d)). The liquid sloshes from left to right and the chaotic motions can best be appreciated by viewing the animations on our web site http://ct-cr4.chem.uva.nl/oil-water. The time- and azimuthal-averaged profiles for $h = 1.6$ m are shown in Fig. 3. The time-averaged $V_L(r)$ is in good agreement with the measurements of Krishna et al. (1999b, 2000). We note in Fig. 3 that the small bubbles tend to concentrate near the wall region whereas the large bubbles predominate in the central core.

Fig. 4(a) compares the experimental $V_L(r)$ profile for air–water and air–Tellus oil (measured by Krishna et al., 2000) with the 3D simulations. Though the two liquids differ in viscosity by a factor 75, both experiments and 3D simulations show almost no influence of viscosity on $V_L(r)$. The centre-line liquid velocity $V_L(0)$ predicted by the 3D and 2D axi-symmetric simulations were close to one another and both in reasonable agreement with experiments (see Fig. 4(b)).

Fig. 5(a) shows a typical response to the salt tracer experiments of Krishna et al. (1999b). Fig. 5(b) shows a typical response from a 3D simulation. The responses at the three monitoring stations can be fitted to a one-dimensional model (Eqs. (12) and (13)) to obtain the value of $D_{ax,L}$. Fig. 5(c) compares the response in the homogeneous flow regime ($U = 0.034$ m/s) with that in the heterogenous flow regime. The latter shows a much stronger dispersion. The values of $D_{ax,L}$ obtained by fitting the response curves shown in Fig. 5(b) are compared with experimental data in Fig. 6. There is reasonably good agreement between the experimental data and the 3D simulations (both conforming to a simple empirical formula $D_{ax,L} = 0.31\ V_L(0)\ D_T$). The 2D simulations, however, yield $D_{ax,L}$ values about one order of magnitude lower than those found experimentally. This limitation of the 2D simulations to represent the mixing characteristics in bubble columns has been underlined earlier by Bauer and Eigenberger (1999).

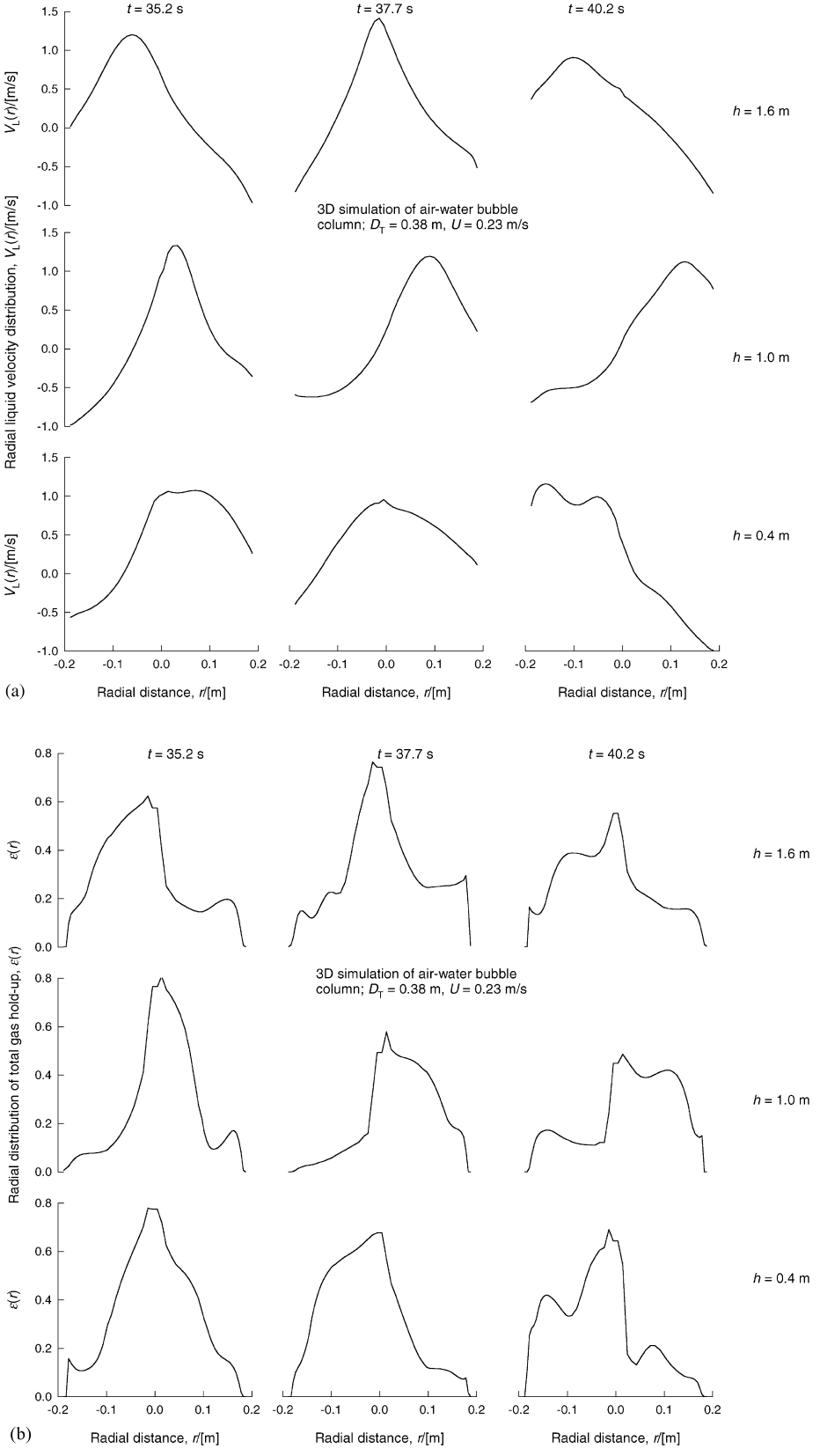

Fig. 2. (a) Radial profiles of liquid velocity. Snapshots at three time steps and at the three monitoring stations in Fig. 1(c). Column diameter = 0.38 m; air–water system, $U = 0.23$ m/s. The animations of this simulation can be viewed on our web site: http://ct-cr4.chem.uva.nl/oil–water. (b) Radial profiles of total gas hold-up for the same conditions as for Fig. 2 (a). (c) Radial profiles of large bubble hold-up for the same conditions as for Fig. 2 (a). (d) Radial profiles of small bubble hold-up for the same conditions as for Fig. 2 (a).

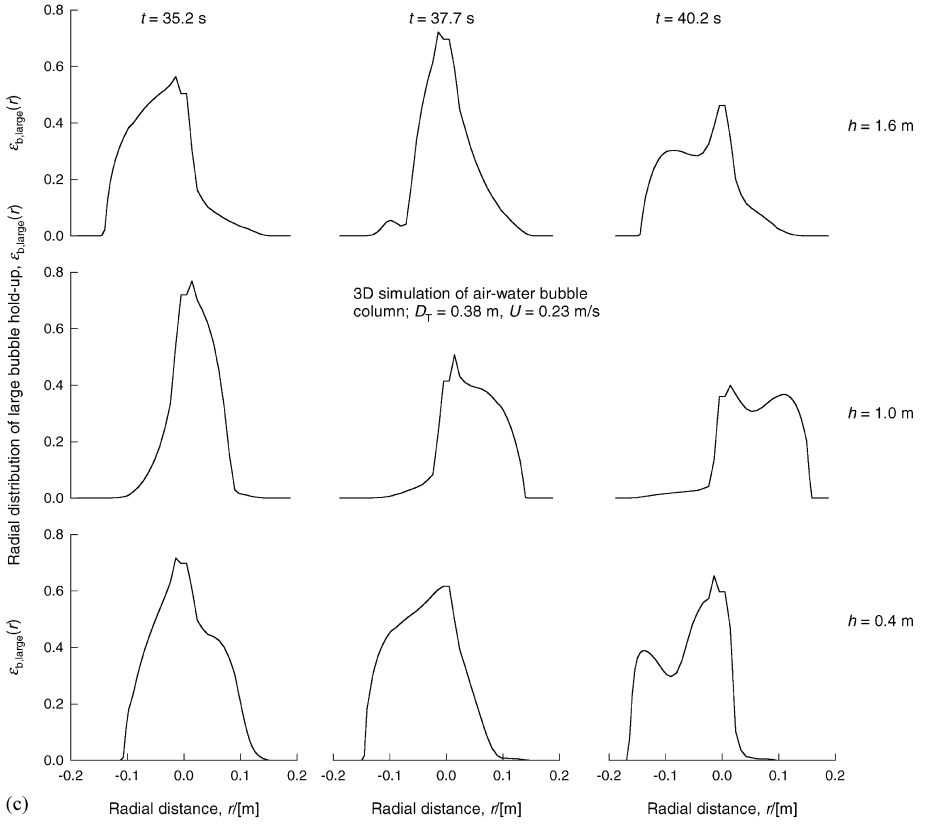

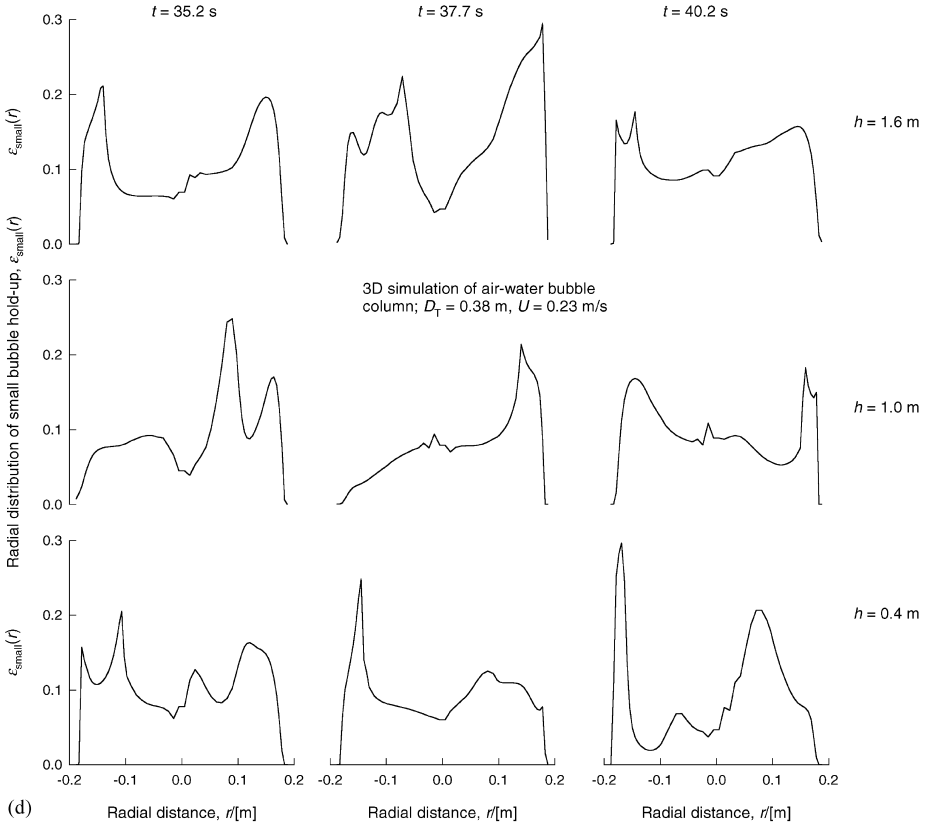

Fig. 2 (continued).

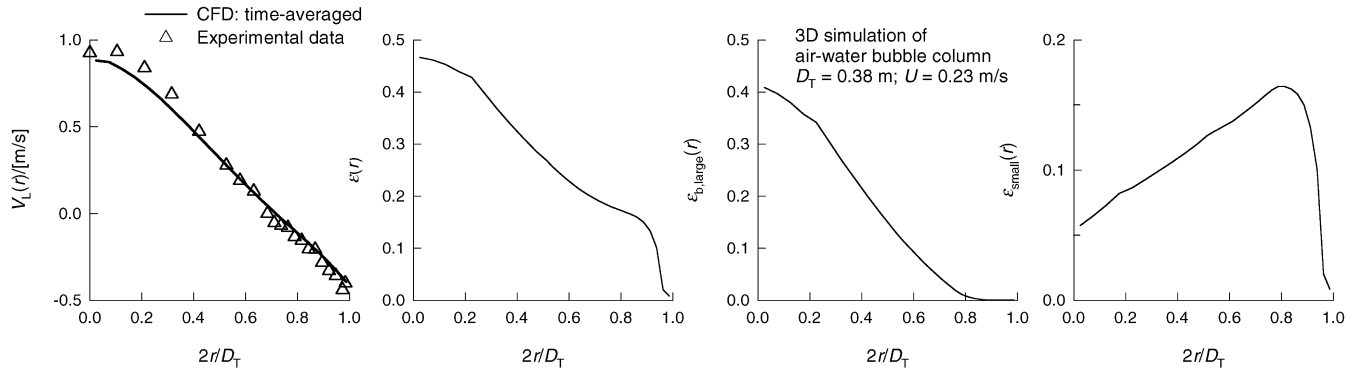

Fig. 3. Time- and azimuthal-averaged radial profiles of liquid velocity (triangular symbols denote experimental data), total gas hold-up, large bubble hold-up and small bubble hold-up. Column diameter = 0.38 m; air–water system, $U = 0.23$ m/s.

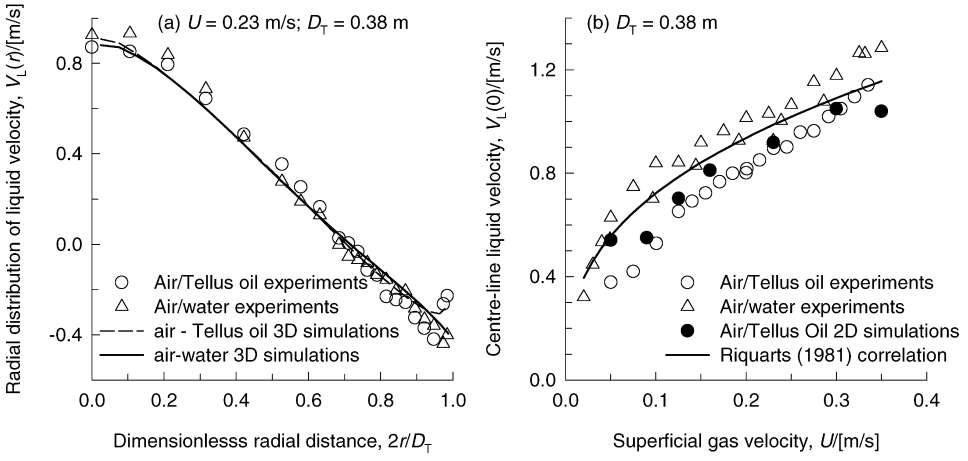

Fig. 4. (a) Time-averaged radial distribution of liquid velocity. Experimental data for air–water and air–Tellus oil compared with 3D Eulerian simulations. (b) Centre-line liquid velocity for air–water and air–Tellus oil compared with 2D Eulerian simulations for air–Tellus oil.

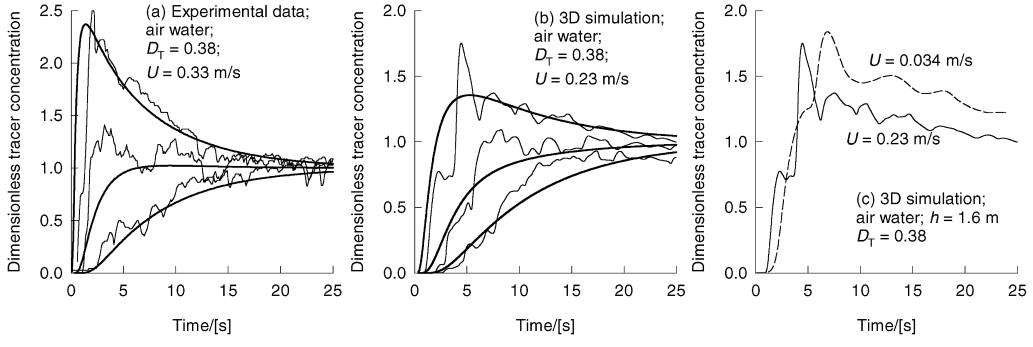

Fig. 5. (a) Dimensionless salt concentration measured at three different monitoring stations in the experiments of Krishna et al. (1999b). (b) Dimensionless tracer concentration from 3D Eulerian simulations for $U = 0.23$ m/s. (c) The tracer response for $U = 0.23$ m/s compared with that of a homogeneous run at $U = 0.034$ m/s.

The response to the gas tracer experiments is shown in Fig. 7, separately for (a) large bubbles, (b) small bubbles and (c) total gas. In the churn-turbulent regime, the total gas RTD shows a camel-hump-shaped curve, reported earlier in the experiments of Vermeer and Krishna (1981). Such a curve is not amenable to interpretation in terms of an axial dispersion model, Eqs. (14) and (15). Fig. 7(c) shows clearly the differences between the gas phase RTD in the homogeneous ($U = 0.034$ m/s) and churn-turbulent flow regime. The responses of the large and

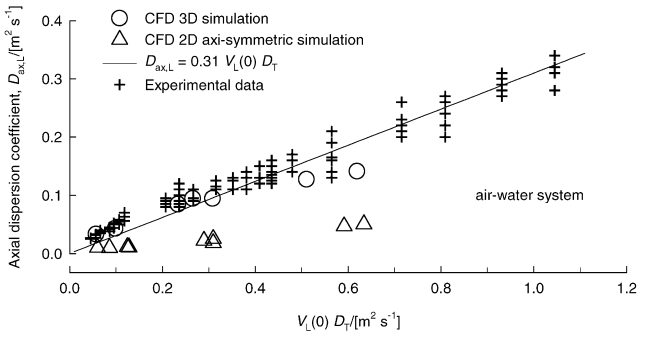

Fig. 6. Axial dispersion coefficient of the liquid phase. Comparison of experimental data of Krishna et al. (1999b) with 2D and 3D Eulerian simulations.

4. Concluding remarks

The predictions of radial distribution of liquid velocity $V_L(r)$ from 3D Eulerian simulations are in good agreement with experiment. Both experiment and simulations show a negligible influence of liquid viscosity on the $V_L(r)$. The liquid-phase axial dispersion coefficient $D_{ax,L}$ predicted from 3D simulations are in good agreement with experiment. Two-dimensional axi-symmetric simulations lead to significantly lower predictions.

In the churn-turbulent regime, the total gas phase RTD is not amenable to interpretation in terms of an axial dispersion model. The individual bubble phase RTD have to be fitted separately. The small bubble

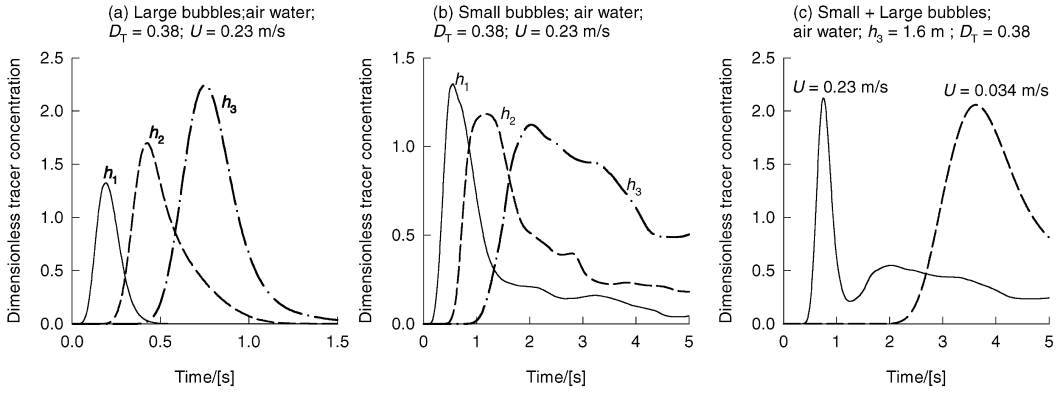

Fig. 7. Dimensionless gas-phase tracer concentrations a three monitoring positions. 3D Eulerian simulations for 0.38 m diameter column. (a) Large bubble response, (b) small bubble response and (c) total gas response.

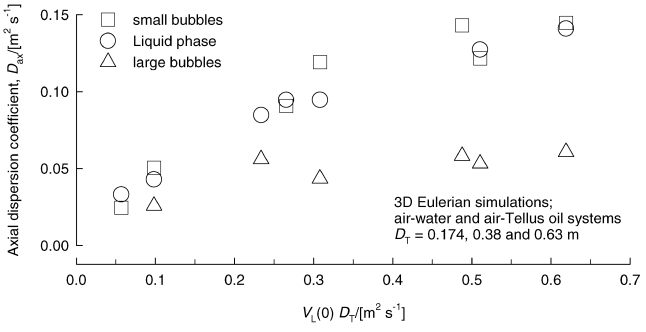

Fig. 8. Axial dispersion coefficient of the liquid phase and gas phase (small and large bubbles) obtained from 3D simulations.

small bubble populations, fitted separately to obtain $D_{ax,G,large}$ and $D_{ax,G,small}$, are compared with the simulated $D_{ax,L}$ values in Fig. 8. The $D_{ax,G,small}$ are remarkably close to $D_{ax,L}$; this assumption has been incorporated into the bubble column slurry reactor model of Krishna and Sie (2000). The dispersion of the large bubbles is significantly lower.

$D_{ax,G,small}$ was found to be remarkably close in value to $D_{ax,L}$ suggesting that the small bubbles are "entrained" with the liquid phase and have similar backmixing characteristics. The dispersion of the large bubbles is significantly smaller.

In view of the success achieved in modelling the dispersion characteristics of columns of three different diameters, we venture to suggest that Eulerian simulations could be used for scale-up purposes for commercial reactor design.

Notation

AF	acceleration factor, dimensionless
d_b	diameter of either bubble population, m
c	tracer concentration, arbitrary units
C_D	drag coefficient, dimensionless
D_{ax}	axial dispersion coefficient, m^2/s
D_T	column diameter, m
$Eö$	Eötvös number, $g(\rho_L - \rho_G)d_b^2/\sigma$
g	acceleration due to gravity, 9.81 m/s^2

h height above distributor, m
$\mathbf{M}$ interphase momentum exchange term, N/m^3
p pressure, N/m^2
Pe Peclet number, defined in Eq. (15)
r radial coordinate, m
SF scale correction factor, dimensionless
t time, s
$\mathbf{u}$ velocity vector, m/s
U superficial gas velocity, m/s
V_b rise velocity of bubble population, m/s
$V_L(r)$ radial distribution of liquid velocity, m/s
$V_L(0)$ centre-line liquid velocity, m/s
x distance from the distributor, m

Greek letters

ε volume fraction of gas phase, dimensionless
μ viscosity of phase, Pa s
r density of phases, kg/m^3
σ surface tension of liquid phase, N/m

Subscripts

b referring to large bubble population
G referring to gas phase
k index referring to either gas or liquid phase
large referring to large bubbles
L referring to liquid phase
s referring to solid catalyst particles
small referring to small bubbles

Acknowledgements

Financial assistance from The Netherlands Organization for Scientific Research (NWO) in the form of a "programmasubsidie" to RK is gratefully acknowledged. JMvB is also grateful to NWO for grant of a Ph.D. fellowship.

References

Bauer, M., & Eigenberger, G. (1999). A concept for multi-scale modeling of bubble columns and loop reactors. *Chemical Engineering Science*, *54*, 5109–5117.

Collins, R. (1967). The effect of a containing cylindrical boundary on the velocity of a large gas bubble in a liquid. *Journal of Fluid Mechanics*, *28*, 97–112.

Deckwer, W. D. (1992). *Bubble column reactors*. New York: Wiley.

De Swart, J. W. A., Van Vliet, R. E., & Krishna, R. (1996). Size, structure and dynamics of "large" bubbles in a 2-D slurry bubble column. *Chemical Engineering Science*, *51*, 4619–4629.

Harmathy, T. Z. (1960). Velocity of large drops and bubbles in media of infinite or restricted extent. *American Institute of Chemical Engineers Journal*, *6*, 281–288.

Jakobsen, H. A., Sannæs, B. H., Grevskott, S., & Svendsen, H. F. (1997). Modeling of bubble driven vertical flows. *Industrial and Engineering Chemistry Research*, *36*, 4052–4074.

Krishna, R. (2000). A scale up strategy for a commercial scale bubble column slurry reactor for Fischer Tropsch synthesis. *Oil and Gas Science and Technology, Revue de L'Institut Francais du Petrole*, *55*, 359–393.

Krishna, R., & Ellenberger, J. (1996). Gas hold-up in bubble column reactors operating in the churn-turbulent flow regime. *American Institute of Chemical Engineers Journal*, *42*, 2627–2634.

Krishna, R., Ellenberger, J., & Sie, S. T. (1996). Reactor development for conversion of natural gas to liquid fuels: A scale up strategy relying on hydrodynamic analogies. *Chemical Engineering Science*, *51*, 2041–2050.

Krishna, R., & Sie, S. T. (2000). Selection, design and scale-up aspects of Fischer–Tropsch reactors. *Fuel Processing Technology*, *64*, 73–105.

Krishna, R., Urseanu, M. I., van Baten, J. M., & Ellenberger, J. (1999a). Rise velocity of a swarm of large gas bubbles in liquids. *Chemical Engineering Science*, *54*, 171–183.

Krishna, R., Urseanu, M. I., van Baten, J. M., & Ellenberger, J. (1999b). Influence of scale on the hydrodynamics of bubble columns operating in the churn-turbulent regime: Experiments vs. Eulerian simulations. *Chemical Engineering Science*, *54*, 4903–4911.

Krishna, R., Urseanu, M. I., van Baten, J. M., & Ellenberger, J. (2000). Liquid phase dispersion in bubble columns operating in the churn-turbulent flow regime. *Chemical Engineering Journal*, *78*, 43–51.

Krishna, R., & van Baten, J. M. (1999). Simulating the motion of gas bubbles in a liquid. *Nature*, *398*, 208.

Krishna, R., van Baten, J. M., & Urseanu, M. I. (2000). Three-phase Eulerian simulations of bubble column reactors operating in the churn-turbulent flow regime: A scale up strategy. *Chemical Engineering Science*, *55*, 3275–3286.

Maretto, C., & Krishna, R. (1999). Modelling of a bubble column slurry reactor for Fischer Tropsch synthesis. *Catalysis Today*, *52*, 279–289.

Mendelson, H. D. (1967). The prediction of bubble terminal velocities from wave theory. *American Institute of Chemical Engineers Journal*, *13*, 250–253.

Reilly, I. G., Scott, D. S., De Bruijn, T. J. W., & MacIntyre, D. (1994). The role of gas phase momentum in determining gas hold-up and hydrodynamic flow regimes in bubble column operations. *Canadian Journal of Chemical Engineering*, *72*, 3–12.

Sanyal, J., Vasquez, S., Roy, S., & Dudukovic, M. P. (1999). Numerical simulation of gas–liquid dynamics in cylindrical bubble column reactors. *Chemical Engineering Science*, *54*, 5071–5083.

Sie, S. T., & Krishna, R. (1999). Fundamentals and selection of advanced Fischer–Tropsch reactors. *Applied Catalysis A*, *186*, 55–70.

Sokolichin, A., & Eigenberger, G. (1999). Applicability of the standard – turbulence model to the dynamic simulation of bubble columns: Part I. detailed numerical simulations. *Chemical Engineering Science*, *54*, 2273–2284.

Vermeer, D. J., & Krishna, R. (1981). Hydrodynamics and mass transfer in bubble columns operating in the churn-turbulent regime. *Industrial and Engineering Chemistry Process Design and Development*, *20*, 475–482.

Westerterp, K.R., van Swaaij, W.P.M., & Beenackers, A.A.C.M. (1984). *Chemical reactor design and operation*, (p. 191). Chichester, UK: Wiley.